Computational Materials Science 253 (2025) 113866

Contents lists available at ScienceDirect

Computational Materials Science

journal homepage: www.elsevier.com/locate/commatsci

Full Length Article

Atomistic molecular dynamics simulations of the tensile strength properties of polymer-calcite systems

Keat Yung Hue [a,c], Daniela Andrade Damasceno [b], Myo Thant Maung Maung [c], Paul F. Luckham [a], Omar K. Matar [a], Erich A. Müller [a,*]

[a] Department of Chemical Engineering, Imperial College London, London SW7 2AZ, UK
[b] Department of Mechatronics and Mechanical Systems Engineering, University of São Paulo, Av. Professor Mello Moraes, 2231, São Paulo 05508-030 SP, Brazil
[c] PETRONAS Research Sdn. Bhd., Lot 3288 & 3289, Off Jalan Ayer Itam, Kawasan Institusi Bangi, 43000 Kajang, Selangor, Malaysia

ARTICLE INFO

Keywords:
Atomistic molecular simulation
Tensile deformation
Solid–fluid interaction
Surfaces
Polymers

ABSTRACT

The production of solids can occur in poorly consolidated carbonate rock reservoirs, leading to equipment damage and environmental waste. This issue can be mitigated by injecting formation-strengthening chemicals, and the performance of these chemicals can be assessed in terms of their tensile strength and interfacial interaction with calcite, the main component of carbonate formations. This study aims to investigate the tensile deformation behaviour of polymer-calcite systems. Classical atomistic molecular dynamics (MD) simulations are utilised to model the interaction of polyacrylamide-based polymer additives, including pure polyacrylamide (PAM), hydrolysed polyacrylamide (HPAM), and sulfonated polyacrylamide (SPAM) with a calcite (1 0 4) structure. Uniaxial tensile simulations demonstrate that the interfacial strength of the polymer-calcite system is significantly stronger than the corresponding bulk polymer strength, resulting in strong polymer adhesion at the calcite surface during deformation. HPAM exhibits high bulk polymer and interfacial strength, presumably due to the presence of the acrylate monomer in ionised form, making it an excellent formation-strengthening agent.

1. Introduction

In reservoir formations, the term formation strength describes the mechanical strength property that holds and adheres the formation grain together in rock reservoirs. Solids production is a problem that can occur when the induced formation stress exceeds the formation strength, particularly for weak and poorly unconsolidated carbonate reservoirs [1]. This can cause solid particles to dislodge from the formation and be transported along with the reservoir fluid, potentially leading to surface equipment clogging and increasing environmental waste. A formation-strengthening chemical is typically applied to enhance the intergranular forces between formation grains, thereby reducing the risk of solids production.

Polyacrylamide-based (PAM) polymers are potential candidates for this purpose, due to their excellent viscosifying properties [2]. They have been utilised as flocculation agents in wastewater treatment and gelling agents in energy applications [3,4]. PAMs can be easily synthesised and hydrolysed with different copolymers, such as hydrolysed polyacrylamide (HPAM) to form a carboxylic acid group, or sulfonated polyacrylamide (SPAM), which has a bulkier copolymer of deprotonated 2-acrylamide-tertiary-butyl sulfonic acid [4,5]. Experimental studies have determined the optimal conditions for applying PAM-based polymers in both sandstone and carbonate formations [2,3,6–8].

Screening the wide range of possible alternative chemistries and polymer morphologies through experiments is time-consuming and ineffective. It is here where molecular modelling can have an edge in designing new materials and exploring material properties. It can facilitate chemical screening by identifying potential candidates to support experimental synthesis. In our previous work [9,10], we described the adsorption behaviour of PAM-based polymers on calcite surfaces, focusing on the molecular adsorption mechanism, binding energies, and the influence of varying reservoir conditions and polymer chemistries. Building on this foundation, the current study shifts its focus to mechanical strength, aiming to investigate the tensile strength properties of PAM-based polymers with calcite surfaces under deformation.

While extensive literature exists relevant to PAM polymer or calcite systems [11–16], the application of tensile simulation studies to these

* Corresponding author.
E-mail address: e.muller@imperial.ac.uk (E.A. Müller).

https://doi.org/10.1016/j.commatsci.2025.113866
Received 12 November 2024; Received in revised form 12 February 2025; Accepted 23 March 2025
Available online 1 April 2025

systems has not been explored. To provide a comprehensive background on tensile simulations, the next section will provide an overview of mechanical strength studies, a discussion of key parameters affecting the tensile strength of various polymer-surface systems, and a highlight of studies closely related to mechanical properties or tensile simulations involving calcite surfaces or PAM systems.

1.1. Tensile simulation studies

The mechanical response of a material refers to the internal structural changes under external forces [17], with uniaxial tensile deformation serving as a well-established technique to assess the material properties under extreme loading conditions [18]. In composite materials, the characterisation of the interface performance and adhesion strength can also be evaluated using tensile pull-off tests [17,19] to determine whether the failure occurs at the interface (adhesive failure) or within the individual phase with weaker resistance (cohesive failure).

Although experimental methodologies are practical and effective for characterising interfacial properties, most techniques are destructive and are typically costly. MD simulations are a powerful tool for designing and predicting composite material performance. Given that the interfacial properties can be governed by the intermolecular interaction of the material with different chemical compositions, MD simulations can reveal mechanical behaviour at the atomistic scale and provide insights into the relationship between chemical structures and properties of interest (see **section S1** in **Supplementary Information**).

MD simulations have been utilized to explore the interfacial strength or adhesion performance of bilayer systems in various fields, such as electronic packaging [20], food packaging [21], the cement industry [22–24], and polymer nanocomposites research [25–30]. Studies typically involve placing a polymer matrix on a mineral surface, mimicking the experimental realization. The results report how polymer chain and system size configuration [21,22,25,28,31], types of surface or polymer functional groups [21,22,24,26,27,30], temperature [19,20,27], and strain or loading rate [19,20,24,27,28,30] affect the deformation mechanism and interface failure behaviour.

1.1.1. Parameter effects on tensile strength of different polymer-surface systems

Perhaps the most frequently studied cases in the literature regarding polymer interfacial deformation are polyethene (PE) with different surfaces, notably silica [22], alumina [21] and graphene/carbon nanotubes (CNT) [25,26,31–33]. This polymer can be applied as a cementitious composite to control cement crack width or augmented with different nanofillers to enhance mechanical, electrical, and thermal properties. Consequently, research has focused on investigating the interfacial properties within these binary systems.

Nikkhah et al. [25] examined the impact of polymer chain composition by exploring the tensile simulation of PE/graphene systems with stress-displacement responses, interfacial energy and energy decomposition analysis. Their findings suggested that both the length of PE chains and the number of chains influence tensile strength and interface failure. When the polymer chain falls below a critical entanglement length, cohesive failure occurs, whereas adhesive failure is observed when the polymer chain surpasses this threshold. The researchers proposed that increased polymer chain length and quantity elevate the probability of chain entangling, augmenting molecular interactions within the polymer bulk interphase. In contrast, Zhou et al. [22] reported similar effects of these parameters on tensile strength on the PE/silica system. However, polymer separation consistently occurred at the bulk region regardless of increasing polymer chain length and number. In this case, the silica surface was modified with coupling agents, leading to enhanced adhesion and tensile strength in the PE/silica system. Olsson and Bergvall [21] investigated the PE/alumina system and observed that the tensile strength remained unchanged despite polymer system size variations and functionalisation. These contradictory observations regarding the effect of polymer system size on tensile strength have also been reported in studies by Zhang et al. [33] and Awasthi [31] on PE/graphene systems, where a slight decrease in tensile strength was observed with increasing system size, eventually converging to a consistent value. This suggests that the influence of the polymer chain and system size on tensile strength may be affected by the simulation protocol or by the specifics of the polymer-surface interfaces. In this context, Yuan et al. [30] assessed the interfacial strength of PE, polyurethane and polystyrene with both regular graphene and functionalised graphene interfaces. They inferred that a higher ratio of interfacial strength to bulk polymer strength leads to a stronger interface, with separation occurring primarily at the bulk polymer region. Similarly, Jose et al. [27] studied the polyisoprene/silica and polyisoprene/graphene interfaces, finding that the bulk polymer strength is affected by the interfacial strength.

Meanwhile, the impact of temperature on tensile strength appears consistent across different studies. With elevating temperature, the polymer phase undergoes softening and higher mobility, facilitating easier chain sliding, reduced resistance to deformation, and consequently lower tensile strength [19,20,27].

The tensile strength and Young's modulus typically increase with strain rate, while the behaviour of polymer-surface separation can vary across different strain rates [27]. Higher tensile strength with increasing strain rate has been reported in various polymer-surface systems, including PE [30], polypropylene [28], high molecular weight methacrylate (HMWM) [24] and asphalt binder [19]. The selection of strain rate depends on the specific property of interest. For instance, Modi et al. [28] found that an intermediate strain rate provided the most accurate representation of mechanical properties in the polypropylene/cellulose nanofibrils (CNF) system. However, this trend of strain rate effect on tensile strength may not always hold for all polymer systems. Yang et al. [20] investigated the epoxy moulding compound/copper system and observed that the strain rate had no discernible effect on tensile strength. Notably, the stress–strain response of this polymer system also differed from that of others reported in the literature. In most polymer-surface tensile simulations, stress reaches a peak value in the yielding region and gradually reduces to zero in the post-yielding region. In the case of the epoxy polymer-copper system studied by Yang et al., there was a strain-hardening region in the post-yielding phase, where the ultimate tensile strength was observed as a secondary peak after the yield strength, and polymer separation occurred at the interface. This implies that the effects of strain rate and the stress–strain response in certain polymer systems might differ from the general trend.

1.1.2. Literature on mechanical properties of PAM-calcite system

Limited literature exists regarding the atomistic tensile simulation of polyacrylamide (PAM) and calcite system. Boudraa et al. [29] constructed interpenetrating polymer networks of PAM and polyacrylic acid (PAA) with varying compositions and subjected them to tensile deformation, where they observed the addition of PAA into the PAM network improved the strength of the overall system. Ji and Arson [24] conducted tensile simulations of high molecular weight methacrylate (HMWM) with silica and calcite systems to compare the interfacial strength of different mineral surfaces. They found that polymer separation occurred at the interfaces in both systems, with the interfacial strength of HMWM/silica being stronger. Furthermore, some simulation research concentrated solely on the mechanical properties of polymers systems. Demianeko et al. [34] investigated the mechanical properties and elastic constants of pure PAM systems for biomedical hydrogel applications. Wei et al. [35] studied a polymer blend system consisting of PAM and polyvinyl alcohol (PVA), noting that the mechanical properties of the system improved with increasing PVA composition due to enhanced interactions among PVA chains. In a follow-up study, Wei et al. [36] incorporated nano silica into the PVA/PAM system and conducted shear simulations, observing further improvements in mechanical properties and internal binding strength due to the formation of

hydrogen bonding.

Experimentally, introducing reinforcing agents such as multiwall carbon nanotubes and cellulose nanocrystals to enhance PAM-based hydrogels has also been explored, showing improvements in mechanical properties [37,38]. Incorporating $CaCO_3$ into PAM/PVA hydrogels has demonstrated improved cross-linking density and mechanical robustness, contributing to enhanced tensile and fatigue resistance [39]. In addition, the *in-situ* formation of amorphous calcium carbonate within PAM hydrogels has been reported to significantly enhance their mechanical properties, with a 13-fold increase in fracture energy and up to a 50-fold increase in stiffness when PAM is functionalised with acrylic acid [40]. Moreover, the functionalisation of PAM with acrylic acid or chitosan microcrystalline structures has led to significant increases in stiffness and toughness [41].

In summary, although numerous studies have investigated tensile simulations of polymer surfaces, there exists a significant gap in research concentrating on the PAM-based polymer-calcite interfacial system. Assessing the interfacial strength of various PAM-based polymers could provide insights into their strengthening performance. Furthermore, conflicting responses have been observed even within the same type of polymer system. [30,42].

In this study, the mechanical strength properties of the polymer-calcite system will be studied using atomistic molecular dynamics simulations. Different simulation protocols are developed to examine the polymer's bulk strength and the polymer-calcite system's interfacial strength. The effects of polymer chain configuration and functional groups of different PAM-based polymers are also evaluated to determine the polymer candidate with the best formation-strengthening performance. For completeness, the results obtained for PAM-based polymers will be compared to those of PE, as PE is one of the most extensively studied polymers.

2. Methodologies

2.1. Simulation details

Classical atomistic molecular dynamics (MD) simulations are employed using the Material Exploration and Design Analysis (MedeA) simulation software [43] integrated with the LAMMPS module [44] with a custom-made visualisation interface. All the molecules in the system are atomistic and are described using the enhanced version of the all-atom Polymer Consistent Force Field (PCFF+) actively developed by MedeA. We note that the results of the simulations are heavily reliant on the choice of the force field, underscoring the importance of defining and validating the force field [45]. As detailed in our previous work [9], the PCFF + force field was validated by comparing simulation outcomes, such as calcite structural properties, adsorption energies of organic compounds and adsorbates on calcite surfaces, with experimental and literature data. The reader is referred to our previous work [9] for the relevant details. The force field cut-off distance is kept at 9.5Å, and treatment of the long-range electrostatic interaction is via the particle–particle–particle Mesh (PPPM) method [46]. System minimisation is performed using the conjugate gradient method, and the simulations are conducted with the velocity Verlet algorithm with a timestep of 1 fs. Periodic boundary conditions are applied in all Cartesian directions. The system is controlled using the Nosé-Hoover thermostat and barostat with the correction terms of Martyna, Tuckerman, and Klein [44,47] included in the equations of motion.

2.2. Polymer-calcite system configuration

2.2.1. Calcite model

The calcite structure is modelled to represent the carbonate rock. The unit cell is a rhombohedral crystal structure with a space group of $R\,\bar{3}\,c$. It has a dimension of $a = b = 4.980$ Å, $c = 17.192$ Å, and a plane angle of $\alpha = \beta = 90°$, $\gamma = 120°$. It is further cleaved into a crystal plane (1 0 4), which is proven to be the most thermodynamically stable structure and has the lowest surface free energy, as validated in our previous work [9]. The crystal plane is replicated as a 6-layer thickness structure with 720 $CaCO_3$ molecules and dimensions of $a = 48.86$ Å, $b = 49.76$ Å, and $c = 17.84$ Å. Depending on the systems of interest, this 6-layer thickness surface slab may be further divided into two surface slabs, each composed of three layers. This calcite structure will be utilised for systems with varying polymer chain configuration and functional groups, where the calcite atoms are allowed to move freely during the equilibration.

Table 1
Polymer compositions and molecular weight. Here, x and y refer to the ratio of copolymers in a repeat unit.

Polymer	Repeat unit composition	Copolymer ratio	Molecular weight per repeat unit (Da)
PAM	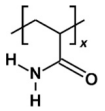	$x = 3$ (repeat unit consists of 3 acrylamide monomeric units)	213.91
HPAM 33%	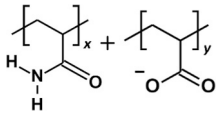	x:y = 2:1	213.89
SPAM 33%	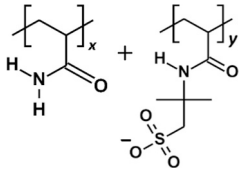	x:y = 2:1	372.06

Table 2
Polymer monomeric units and chain numbers employed to study the effect of polymer chain composition.

Type of polymer	Polymer monomeric units, x	Chain numbers, y
PAM x/y	25	40
	25	80
	50	40
	75	40
	150	20
PE x/y	25	40
	50	40
	200	10

2.2.2. Polymer model

The PAM-based polymers, including basic polyacrylamide (PAM), hydrolysed polyacrylamide with 33% charge density (HPAM 33%), and sulfonated polyacrylamide with 33% charge density (SPAM 33%), are modelled as polymer candidates. The oligomer repeat unit composition and copolymer ratio have been illustrated and detailed in Table 1.

Here, "monomeric unit" refers to the smallest molecule forming a polymer, while "repeat unit" refers to the smallest representative structure forming a copolymerised PAM with a specific copolymer ratio. In the cases of HPAM 33% and SPAM 33%, the repeat unit comprises two acrylamide monomeric units and a deprotonated copolymer group, resulting in a structure with 33% charge density. At the same time, the corresponding size of the repeat unit of pure PAM consists of three acrylamide monomeric units. Given the extensive literature on the tensile simulation of PE polymer, PE is also modelled as a benchmark and comparison case to validate the simulations carried out for PAM-

Table 3
Density of different polymer systems at room temperature range.

Polymers	Density (g/cm^3)		
	Current study	Experimental Literature	Simulation Literature
PAM	1.27–1.28	1.30 [4]	1.23 [49,50], 1.32 [34], 1.34 [35]
HPAM 33%	1.30	–	–
SPAM 33%	1.22	–	–
PE	0.79–0.81	0.91–0.94 [42]	0.78–0.85 [22], 0.82–0.83 [25], 0.87–0.91 [42]

based polymers in the present work.

To investigate the effect of polymer chain composition on the tensile strength of the polymer-calcite system, PAM and PE are modelled with notation using x/y to denote the monomeric units and chain number, as specified in Table 2. This also allows the comparison of the effect of chain number on the deformation behaviour across different polymer types.

Regarding the effect of the polymer functional group, systems with HPAM 33% and SPAM 33% are modelled, each consisting of 8 repeat units per polymer chain and 41 chains for comparison with the PAM 25/40 and PE 25/40 cases. This ensures a similar degree of polymerisation among all the polymers, though there will be some differences in the polymers' molecular weight. Additionally, 328Na^+ ions are included in each HPAM 33% and SPAM 33% system (1 negatively charged segment per repeat unit) to ensure overall system electroneutrality.

2.3. Equilibration of polymer-calcite systems

The equilibration of pure polymer systems is performed first to characterise their densities and compare them with published literature values. For each polymer system, the amorphous polymer is placed randomly within a spacious simulation box with an extended height, maintaining the same cross-sectional area as the calcite surface while the polymer system density is set at 30% of the initial target density ($\rho =$ 1.2 g/cm^3 for PAM, HPAM 33%, SPAM 33%, and $\rho = 0.90$ g/cm^3 for PE) using the MedeA amorphous module. The amorphous system is created without molecules crossing the box boundary in the z-direction to facilitate its subsequent stacking with the calcite surface slab later. Using the MedeA compression module, the amorphous polymer system is gradually compressed to the target density while equilibrating under the $NP_{zz}AT$ ensemble at 300 K, forming a final system with a thin gap layer across the boundary in the z-direction.

In the sequence, the 21-step compression-relaxation scheme of Abbott et al. [48] is employed to equilibrate the amorphous polymer system (see **section S2** in **Supplementary Information** for more equilibration details), where the resulting configuration undergoes simulation annealing from 600 K to 300 K at a cooling rate of 5 K/100 ps over 6 ns and is further equilibrated at 300 K for 5 ns, both under NPT ensemble. **Fig. S2 and S3** in **Supplementary Information** show the time profile of the system's total energy and density during equilibration, confirming that the polymer system is properly equilibrated. The final densities of the polymer systems at room temperature are presented in Table 3, with the density ranges of PAM and PE demonstrating good agreement with those reported in the literature across varying system sizes.

For the equilibration of the polymer-calcite system, the compressed polymer system is initially overlaid with the calcite 6-layer thickness model and equilibrated under $NP_{zz}AT$ ensemble at 300 K and 1 atm to eliminate the gap layer between the polymer-calcite model. A similar equilibration protocol for the pure polymer system is then repeated for the polymer-calcite system. The calcite slab position is adjusted after the equilibration to sandwich the polymer between the 3-layer thickness of the upper and lower calcite slabs. The final system configuration is depicted in Fig. 1, where there is a "vacuum" above the upper slab to allow the expansion of the upper calcite slab without exerting work against the periodic boundary condition in the z-direction, with a vacuum layer thickness of 150 Å added to each polymer-calcite system. The system is further equilibrated using an NVT ensemble at 300 K for 100 ps and prepared for uniaxial tensile deformation.

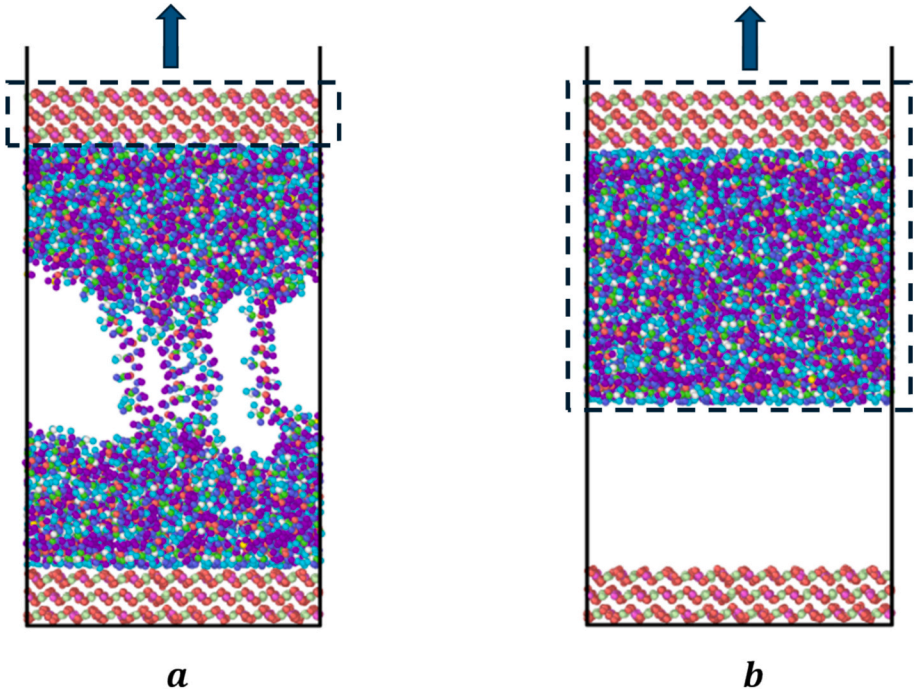

Fig. 1. Uniaxial tensile deformation for two cases: **(a)** the deformable polymer case and **(b)** the rigid polymer case. The dashed line encloses the particles kept rigid ('frozen').

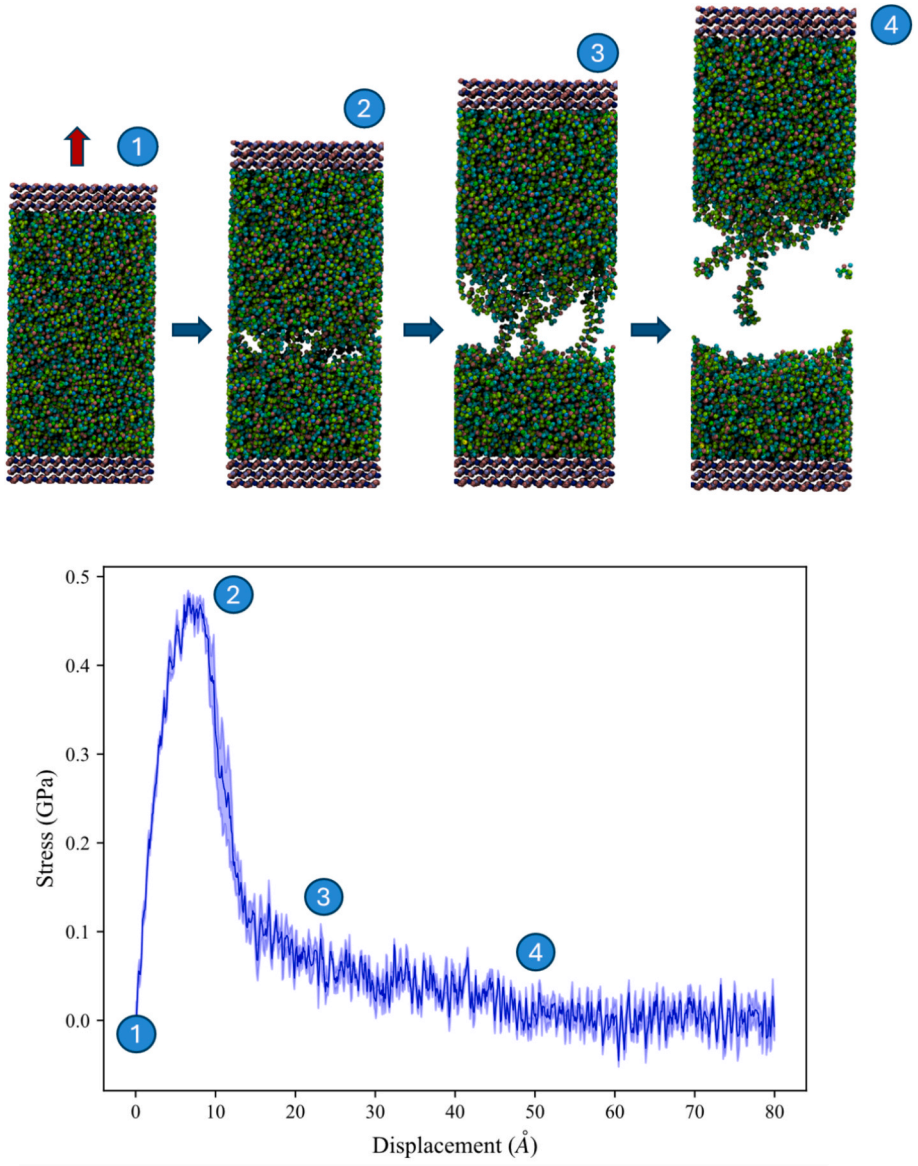

Fig. 2. Uniaxial tensile deformation behaviour for polymer-calcite system PAM 25/80 showing the four distinct regions discussed in the text. The shaded area represents the error bar from 5 different realisations.

2.4. Deformation of polymer-calcite systems

We adapted the simulation workflow from Yuan et al. [30] to quantify the bulk polymer strength and interfacial strength of the polymer-calcite system, where the development of the uniaxial tensile simulation protocol is discussed in **section S3** of the **Supplementary Information**. The uniaxial tensile simulation is performed for two different cases: the deformable polymer case and the frozen polymer case, as depicted in Fig. 1. In the deformable polymer case, only the upper calcite slab layer is kept rigid and pulled upward in the z-direction, allowing the polymer to deform freely under the NVT ensemble at 300 K. Conversely, in the frozen polymer case, both the polymer and upper calcite slab layer are kept rigid and pulled upward together. The tensile simulation is conducted at a displacement rate of 0.0001 Å/fs, equivalent to 10 m/s. This value was chosen based on our preliminary studies (see **Fig. S11** in **Supplementary Information**), considered an intermediate rate [27,28] in simulation studies with reasonable computational efficiency. The deformation is performed for 800 ps, reaching a final displacement of 80 Å for all systems. This study measures the stress-displacement response instead of the stress–strain response, as the chosen displacement rate ensures comparability across varying system sizes. It is important to note that the employed displacement rate is several orders of magnitude higher than that of typical experimental tensile tests, and the measured stress response serves as a qualitative indication only, and a comparative one amongst PAM, HPAM, and SPAM. The stress is measured as the tensile force acting on the bottom calcite layer normalised by the calcite surface area, and the Young's Modulus is computed as a linear stress–strain slope over the elastic regime. For each case, the result computed is averaged over five realisations prepared from system equilibration.

3. Results and discussion

3.1. Deformation mechanism and stress-displacement behaviours

With the developed simulation protocol, we examine the stress-displacement response and deformation mechanism of the deformable PAM-calcite system, considering the PAM 25/80 model. Various stages of deformation related to stress and displacement are illustrated in Fig. 2. During the transition from the initial state (Stage 1) to the

yielding phase (Stage 2), as the calcite slab is pulled upward, the system encounters the applied force and attempts to resist deformation. This resistance manifests itself as a sharp increase in stress in the curve. The region within the interface system exhibiting weaker resistance strength contributes to this stress value, which, in our case, is the bulk polymer region in the polymer-calcite case.

Upon reaching the yielding point, the system can no longer resist the deformation, initiating void formation and the stress reaching its maximum tensile strength. In the post-yielding region (Stage 3), the void sizes continue to grow under tensile loading, causing a drastic decrease in stress following a smooth trend. Deformation behaviour in this stage is typically governed by chain slipping, chain disentanglement, and the tendency of the polymer to detach from the surface. These factors contribute to different trends in the stress reduction curve [21,22,25]. From the literature, if the bulk polymer region exhibits less stiffness and higher mobility, the polymer can easily disentangle and form thinning and channelling during separation. This involvement of the polymer in the deformation mechanism can result in a more erratic stress reduction curve, with the ultimate stress failure reaching a value of 0 at a slower rate.

In the case of PAM-calcite shown in Fig. 2, minimal polymer entanglement is observed with increasing separation, a pattern also noted in polymers with longer chains, such as PAM 75/40 and PAM 150/20 systems (see **Fig. S12** in **Supplementary Information**). For polymer to entangle during traction, the polymers from the initial position in the bulk phase must first disentangle and then re-entangle with other chains during the pulling process. However, due to the branched structure of the PAM and the stronger polar interactions among the chains, the chains strongly intertwine in the initial bulk phase, making separation and disentanglement exceptionally difficult. Consequently, the polymer tends to remain in the same region and in an entangled state, resulting in clean ruptures and polymer separation in the ultimate failure region (Stage 4). Post-deformation is not associated with polymer entanglement and yields a smooth and rapid stress reduction curve. In terms of failure mode, the polymer-calcite system displays cohesive failure, with rupture occurring in the middle bulk region instead of at the interface. This highlights the strong interfacial strength and secure adhesion of the polymer to the calcite surface. For further details on the adsorption mechanism and molecular interactions of the PAM-calcite system, readers are referred to our previous work [9].

3.1.1. Tensile strength analysis

The interpretation of maximum tensile strength from the stress-displacement response can be complex and varies among studies, as it depends on the specific polymer-surface system and simulation protocol. As mentioned, the stress-displacement behaviour of our deformable PAM-calcite system is primarily determined by the bulk polymer strength. A comparative study of a pure polymer system and a polymer-surface system is presented in **Fig. S10** in the **Supplementary Information**.

A similar failure pattern has been noted in other studies. For instance, in the study by Yuan et al. [30] on a polymer-graphene system, it was found that the tensile strength of deformable PE and polystyrene cases matched the pure polymer strength, with cohesive failure observed in the failure region. However, if the polymer-surface interaction is weak and fracture separation occurs near the interface, the peak tensile strength of the deformable polymer case may diverge from the pure polymer strength, as seen in their study of the deformable polyurethane-graphene system.

Other studies have discussed failure occurring at the interface, such as the one conducted by Ji and Arson [24], which focused on a single type of polymer, HMWM, but examined its interaction with different mineral surfaces: calcite and silica. They observed that in both cases, adhesive failure occurred due to weak interfacial strength, resulting in variations in tensile strength across different surfaces. It is worth noting that if adhesive failure occurs at the interface, the peak tensile strength

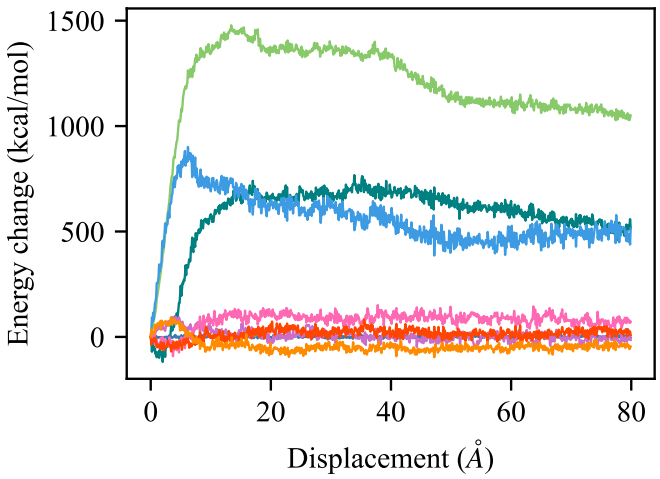

Fig. 3. Energy decomposition analysis for deformable polymer-calcite PAM 25/80 system. Potential energy (light green), van der Waals energy (dark green), coulombic energy (light blue), kinetic energy (dark blue), bond energy (purple), bend angle energy (pink), dihedral energy (red), improper torsional energy (orange). Kinetic energy remains zero energy change throughout tensile displacement. (For interpretation of the references to colour in this figure legend, the reader is referred to the web version of this article.)

in such a system may not necessarily represent the interfacial strength. This is because the peak tensile strength of the polymer-surface system typically occurs at the initial yielding point of the stress-displacement response, whereas adhesive failure only occurs at the failure region in the last stage. Consequently, the peak tensile strength value does not solely reflect the pure interfacial strength. In such scenarios, the tensile strength can be interpreted as a value influenced by both polymer-surface and polymer–polymer interactions, representing the strength required to overcome interface separation and resist deformation within the polymer phase. The dominant factor depends on the type of polymer-surface interaction and the strain rate [27,31]. The interfacial strength is typically analysed using the frozen polymer detachment method [21,30,31] or in terms of energy required to separate the interface per unit of surface area, equivalent to the area under the stress-displacement curve [24,25,27].

Likewise, the behaviour of interface failure modes not directly linked to peak tensile strength implies that in situations where the polymer-surface system undergoes cohesive failure, the peak tensile strength may not consistently reflect the bulk polymer strength. This was observed in the PE-silica system studied by Zhou et al. [22]. Despite all polymer cases remaining adhered to the surface in the failure region, the peak tensile strength of longer polymer chains and functionalised silica surfaces was higher compared to shorter chains and the original silica surface. They explained that longer polymer chains possess greater entanglement strength and surface functionalisation improves interfacial interaction, leading to a higher tensile force transmission to the surface. This results in the interface having stronger energy dissipation and resistance to deformation. Consequently, tensile strength is influenced by both overall cohesive and improved adhesive strength.

In summary, the maximum tensile strength observed in the stress-displacement response may be contributed from both polymer–polymer and polymer-surface interactions and requires careful interpretation. Nevertheless, in our current study, the stress-displacement behaviour of the deformable polymer-calcite system is primarily determined by the bulk polymer strength. Therefore, to quantify the interfacial strength and compare it with the bulk polymer strength, we employ the interfacial strength analysis proposed by Yuan et al. [30], which is discussed using the frozen polymer case in a later section.

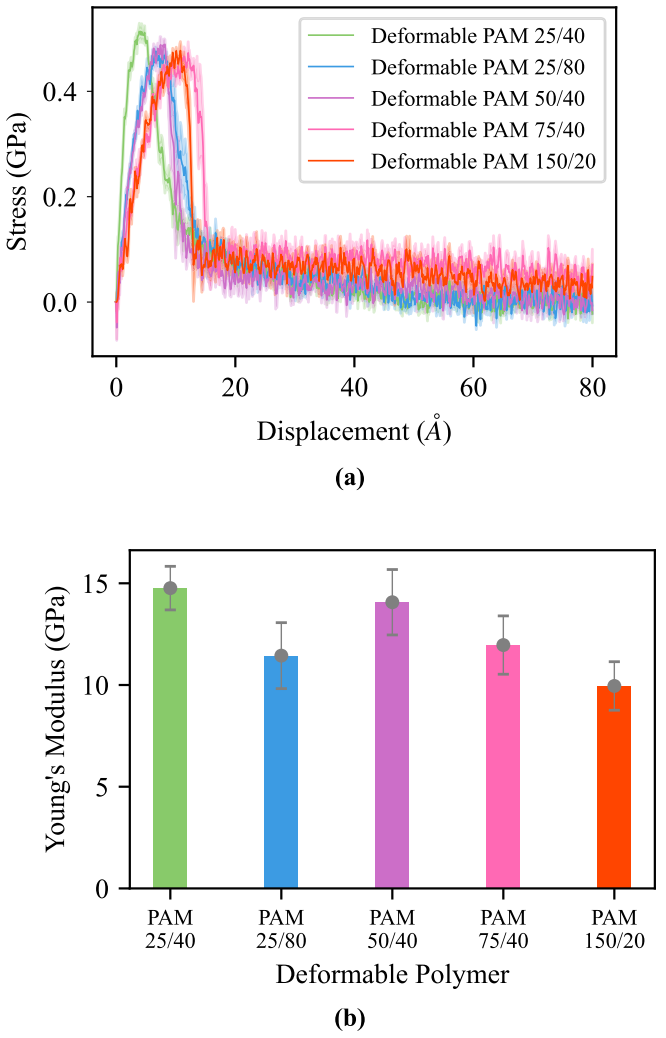

Fig. 4. **(a)** Stress-displacement response and **(b)** Young's Modulus of varying PAM chain composition for deformable polymer cases. Shaded areas and error bars represent standard error from 5 realizations.

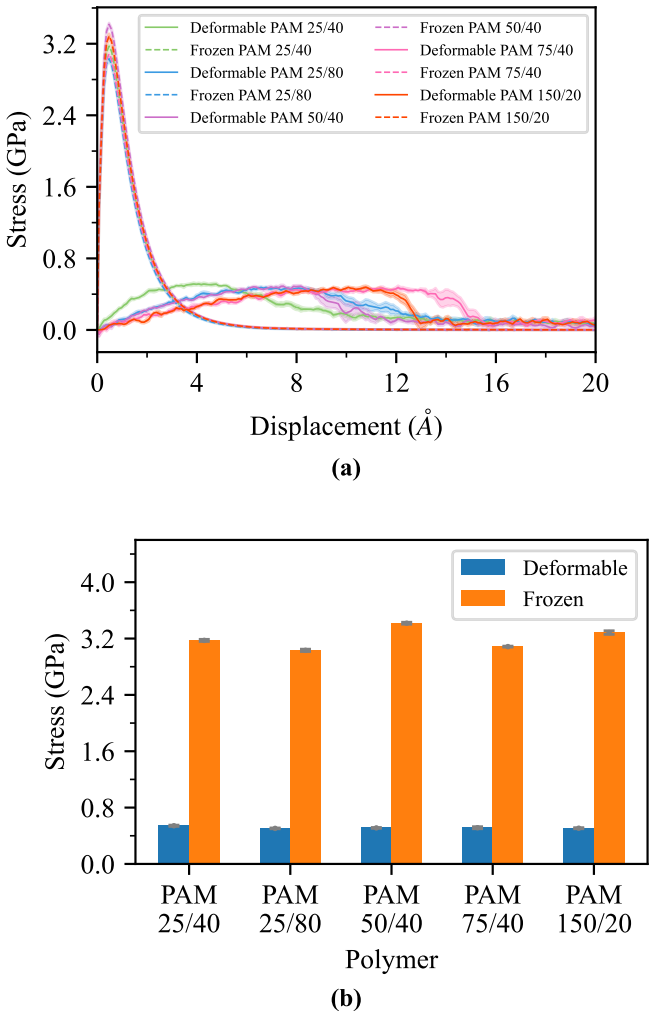

Fig. 5. **(a)** Stress-displacement response and **(b)** Tensile strength of varying PAM chain composition for deformable and frozen polymer cases. The stress-displacement response is zoomed in up to a displacement of 20Å. Shaded areas and error bars represent standard error from 5 realizations.

3.1.2. *Energy decomposition analysis*

The energy decomposition analysis for the tensile simulation of the polymer-calcite PAM 25/80 system is illustrated in Fig. 3. A slight change can be observed in the bonded-interaction energy attributed to stretching bonds, bending angles, dihedrals, and improper torsions from the initial stage to a displacement of 10 Å. This is due to the subtle movement of the polymer with the initiation of void formation and applied tensile force, after which the energy remains unchanged as there is no further polymer rearrangement and rotation.

Meanwhile, the change in non-bonded interaction energy is significantly higher, indicating the dominant role of polymer–polymer and polymer-surface intermolecular interactions during deformation compared to polymer intramolecular movement. The unfavourable increase in overall energy change during deformation is caused by the disruption of the polymer from its initial stable state and its effort to resist the tensile force as displacement from the surface increases, owing to its preference for adhering to the calcite surface due to stronger interfacial interactions. This change corresponds to a sharp increase in the peak tensile strength and stabilises in the post-yielding region. The van der Waals and coulombic interactions contribute equally to the change in non-bonded interaction energy. The shift in energy trend in bonded and non-bonded interaction is similar across all types of polymer systems investigated, except for the PE system (see **Fig. S13** in **Supplementary Information**), where there is no coulombic contribution to the non-bonded interaction energy due to its non-polar nature.

3.2. *Effect of polymer chain composition*

The effect of varying PAM chain monomeric units and chain numbers on the stress-displacement response of deformable polymer cases is presented in Fig. 4**a**, while Young's Modulus is depicted in Fig. 4**b**. Increasing the chain length or chain number in the PAM-calcite system leads to maximum tensile strength and ultimate failure occurring at longer displacements, as more polymers are available to resist the tensile force and deformation. However, the chain composition and size do not significantly affect the tensile strength value and Young's Modulus. The maximum tensile strength consistently falls within the approximate range of 0.46–0.51 GPa, while Young's Modulus remains within the range of 10–16 GPa, aligning with the value of 12.8 GPa reported in the simulation literature [34]. In a tensile test experiment of PAM-cellulose composites, while not focusing on the PAM-calcite system, Voronova et al. [38] reported that pure PAM films had a tensile strength of 56.7 MPa and a Young's modulus of 1.17 GPa. This discrepancy is expected due to the significantly higher pulling rate used in simulations than typical experimental tensile tests [51], with experimental values potentially further influenced by their specific testing conditions.

The negligible effect of chain composition on the tensile strength can be attributed to the polymer's deformation behaviour during tensile

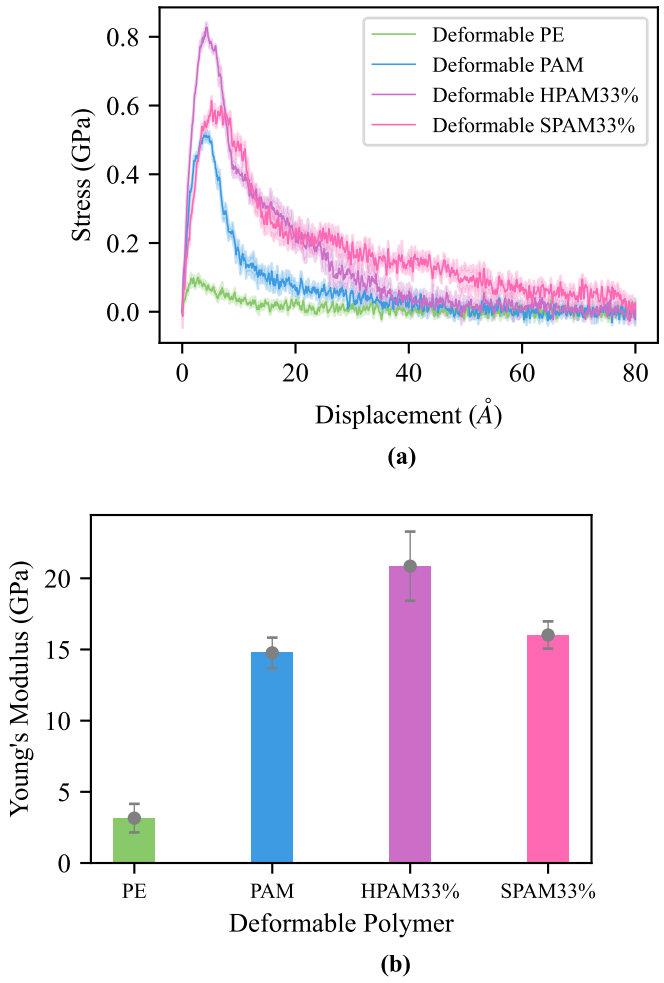

Fig. 6. **(a)** Stress-displacement response and (**b**) Young's Modulus of varying polymer types for deformable polymer cases. Shaded areas and error bars represent standard error from 5 realizations.

simulation. Typically, the tensile strength increases with the polymer with longer chain length, as it increases the probability of polymer channelling with stronger entanglement density [25]. However, our results, including the system with longer chain length and chain number, show minimal polymer channelling connecting the top and bottom regions, with a clean fracture separation occurs during the separation. As mentioned in **section 3.1**, this may stem from the branched nature and strong polar interactions within PAM polymer, where the chain mobility is limited, and the polymer does not disentangle and rearrange itself. Therefore, the minimal effect observed in this study could be attributed to the shorter polymer chains and smaller numbers already entangling strongly within the initial stiff polymer phase. Further increases in chain length and chain number do not enhance the tendency for polymer channelling and, consequently, do not affect the tensile strength. A similar result has been observed by Olsson and Bergvall [21] in their investigation of PE-alumina surfaces with different PE system sizes.

Interestingly, the smallest system PAM 25/40 exhibits slightly higher tensile strength than the larger systems. This could be attributed to system size effects, where increasing the system size leads to a converged response of tensile strength, as supported by the findings of Zhang et al. [33] and Awasthi et al. [31]. This implies that larger systems should be employed for future research to obtain more representative property analysis. Nevertheless, due to computational constraints where each system was simulated five times with a detailed and computationally intensive equilibration process, we decided to use smallest system size in our next section of studying effect of polymer functional groups. This approach is considered acceptable as it can still effectively differentiate and screen different polymer candidates with clear and identifiable bulk polymer and interfacial strengths, therefore maximising computational efficiency.

The stress-displacement response and tensile strength of the deformable polymer case are further compared with the frozen polymer cases, as shown in Fig. 5. In all cases, the interfacial strength spikes to a range of 3.0–3.5 GPa with just a few displacements from the surface. The interfacial strength obtained from the frozen polymer cases is significantly higher than the bulk polymer strength, thereby validating the favourable nature of the polymer-surface interaction and the polymer's ability to adhere to the surface firmly.

Similarly, there is no specific trend of the chain composition's effect on the tensile strength and Young's Modulus of the deformable PE-

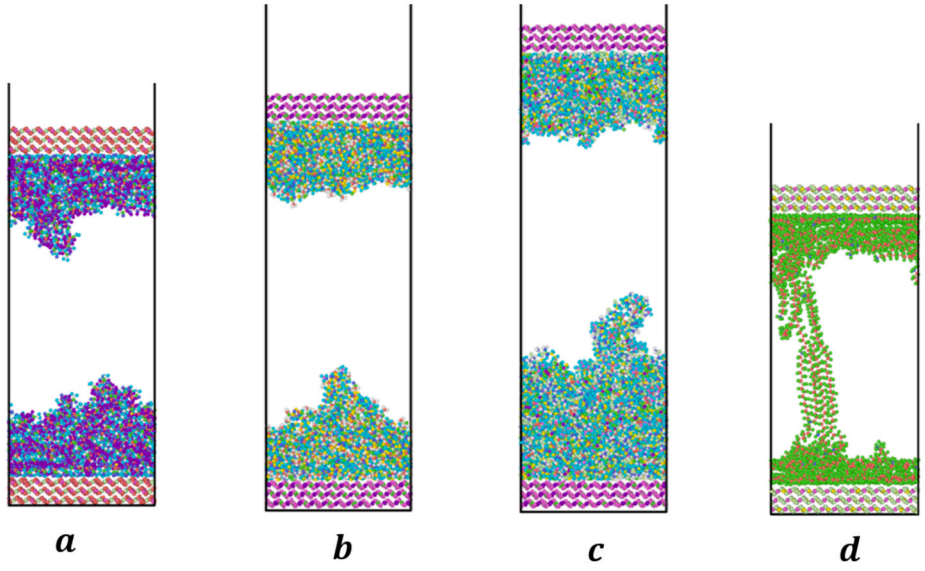

Fig. 7. Simulation snapshots of uniaxial tensile deformation for deformable polymer-calcite system at displacement of 50Å (post-yielding region): **(a)** PAM 25/40, **(b)** HPAM 33%, **(c)** SPAM 33% and **(d)** PE 25/40. Polymers with a similar degree of polymerisation have different initial and final system sizes under the same tensile displacement.

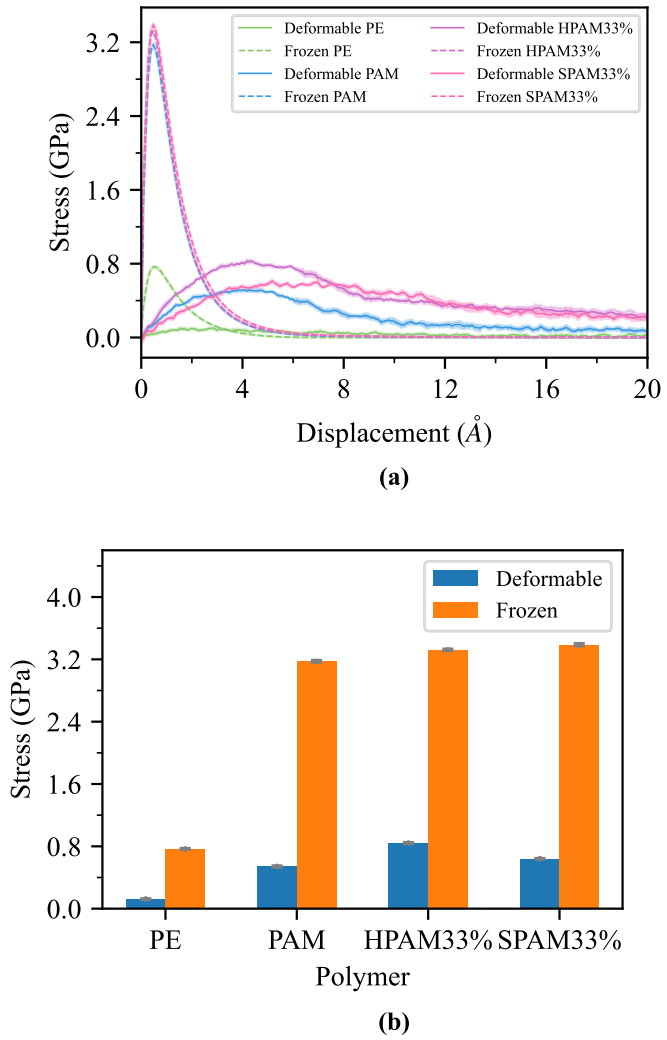

Fig. 8. (a) Stress-displacement response and **(b)** Tensile strength of varying polymer types for deformable and frozen polymer cases. The stress-displacement response is zoomed in up to a displacement of 20Å. Shaded areas and error bars represent standard error from 5 realizations.

calcite system, where the results are presented in **section S6** in **Supplementary Information** as our focus here is on the PAM-calcite system only.

3.3. *Effect of polymer functional groups*

PAM polymer can undergo hydrolysis with various copolymers to enhance viscoelasticity. The tensile behaviour of deformable HPAM 33% and SPAM 33% are depicted in Fig. 6. Although PE is not a potential candidate for formation strengthening, it is included here for comparison with the performance of PAM-based polymers. HPAM 33% exhibits the highest bulk polymer strength and Young's modulus, followed by SPAM 33%, PAM, and PE. This underscores the significance of copolymerisation in enhancing polymer strength performance. The deformation behaviours of all polymers in the post-yielding region are illustrated in Fig. 7. Notably, with a similar degree of polymerisation, copolymerised polymers, especially SPAM 33% with bulkier functional groups will have a larger initial system size.

Under the same tensile displacement, all PAM-based polymers exhibit clean fracture in the post-yielding region. PAM-based polymers can interact among themselves via strong polar interactions. The presence of branched functional groups in the monomer further enhances entanglement and bulk polymer strength, making disentanglement less likely. Comparing HPAM 33% and SPAM, the stronger strength performance of HPAM 33% may be attributed to the deprotonated carboxyl group from the acrylate monomers. The size of this copolymerised functional group is similar to that of the acrylamide monomers, enabling strong interaction and entanglement. Conversely, the bulkier sulfonated copolymer in SPAM 33% has a larger size compared to the acrylamide monomers, where the steric hindrance effect potentially inhibits polar interactions among themselves and results in lower entanglement and tensile strength compared to HPAM 33% [52,53]. However, this also increases the tendency for disentanglement, leading to a slower reduction in stress values to 0 in the post-yielding region compared to HPAM 33%.

In contrast, the PE case shows polymer elongation and channelling during separation before fracturing completely in the failure region, as shown in Fig. 7**d**. Similar elongation behaviour of PE system has also been reported in simulation studies by Nikkhah et al. [25] and Zhou et al. [22]. It is widely recognised that PE is a non-polar molecule lacking a branched structure, and the intermolecular interaction consists solely of van der Waals forces. PE can disentangle and relax more easily among themselves, forming a weaker bulk polymer phase with lower strength.

As depicted in Fig. 8, both HPAM 33% and SPAM 33% exhibit higher interfacial strength than PAM and PE, showcasing superior adhesion performance attributed to stronger electrostatic interaction with the ionic calcite surface. Since the surface is saturated with adhered polymers, the influences of copolymerised functional groups and steric hindrance are insignificant, resulting in similar values between HPAM 33% and SPAM 33%. PE demonstrates the poorest interfacial strength due to relatively weaker interaction with the calcite surface, which is evident from a thinner layer of adherence in Fig. 7**d** compared to other polymers. Based on the tensile simulation analysis of both deformable and frozen polymer cases, HPAM 33% emerges as the most suitable candidate for formation-strengthening performance owing to its stronger interfacial strength and bulk polymer strength to resist deformation.

These findings align with our previously reported adsorption studies [9], indicating that HPAM demonstrates superior adsorption performance compared to SPAM. While the current study focuses on tensile simulations, it is worth noting that unconfined compressive strength (UCS) experimental studies from a collaborative work [7] also exhibit a similar trend to the simulation study: increasing polymer molecular weight shows no effect on compressive strength, and HPAM demonstrates better consolidation strength performance than SPAM. However, given the fundamental differences between tensile simulations and UCS experiments, where UCS measures the compressive strength of consolidated carbonate cores rather than tensile deformation resistance, direct comparisons are impossible. Future studies can employ experimental tensile tests on prepared samples to provide a more direct comparison to the simulation findings.

It is important to emphasise that our tensile simulation uses amorphous polymer at room temperature. Considering that formation-strengthening chemicals are typically injected as aqueous solutions into carbonate formations under challenging reservoir conditions, factors such as high reservoir temperature, the presence of solvent water, and the salinity environment may likely impact the tensile strength of the polymer-calcite system. This presents a potential avenue for future exploration to investigate these related parameters within a more accurate polymer-calcite model.

Furthermore, the tensile strength analysis is conducted on an ideal flat calcite crystal plane, whereas the rock geometry in carbonate reservoirs can be more complicated and irregular. Atomistic simulation faces limitations in modelling irregular calcite surfaces due to their ionic crystal structure. Future research can focus on coarse-grained polymer-calcite system simulation, serving as an alternative approach to model more complex systems with different surface geometries.

4. Conclusions

This study utilised atomistic molecular dynamics simulations to examine the tensile properties and deformation behaviour of polymer-calcite composite materials. We focused on PAM-based polymers, with PE serving as a control. By comparing the tensile strength of pure polymers and polymer-calcite systems, the measured interfacial strength between the polymer and calcite was significantly higher than the bulk strength of the polymer. This strong interfacial interaction led to polymer adsorption onto the calcite surface and eventual failure within the bulk polymer region. Our simulation results indicated that increasing the polymer chain length or number had little impact on tensile strength. Among the PAM-based polymers studied, HPAM exhibited superior bulk and interfacial strength, suggesting it is the most promising candidate for enhancing formation strength and consolidating carbonate formations.

CRediT authorship contribution statement

Keat Yung Hue: Writing – original draft, Investigation. **Daniela Andrade Damasceno:** Validation, Methodology. **Myo Thant Maung Maung:** Supervision, Project administration. **Paul F. Luckham:** Writing – review & editing, Supervision, Conceptualization. **Omar K. Matar:** Writing – review & editing, Supervision, Project administration. **Erich A. Müller:** Writing – review & editing, Supervision, Investigation, Conceptualization.

Declaration of competing interest

The authors declare the following financial interests/personal relationships which may be considered as potential competing interests: Erich A. Muller, Omar K. Matar, Paul F. Luckham reports financial support was provided by PETRONAS Resource Centre. Myo Thant Maung Maung and Hue Keat Yung report relationship with Petroliam Nasional Bhd that includes: employment. If there are other authors, they declare that they have no known competing financial interests or personal relationships that could have appeared to influence the work reported in this paper.

Acknowledgements

We gratefully acknowledge funding from PETRONAS for this work through the PETRONAS Centre for Engineering of Multiphase Systems. DAD thanks the financial support of FAPESP – São Paulo Research Foundation grants 2020/01558–9 and 2022/06973–0.

Appendix A. Supplementary data

Supplementary information is provided with this manuscript, including mechanical properties measurement in MD simulations, equilibration and tensile simulation protocol of polymer-calcite systems, results and discussion of PE-calcite systems, and example input files. Supplementary data to this article can be found online at https://doi.org/10.1016/j.commatsci.2025.113866.

Data availability

Data will be made available on request.

References

[1] M.N.J. Al-Awad, A.-A.-H. El-Sayed, S.-E.-D.-M. Desouky, Factors affecting sand production from unconsolidated sandstone Saudi oil and gas reservoir, J. King Saud Univ. – Eng. Sci. 11 (1999) 151–172, https://doi.org/10.1016/s1018-3639(18)30995-4.

[2] F.S. Alakbari, M.E. Mohyaldinn, A.S. Muhsan, N. Hasan, T. Ganat, Chemical sand consolidation: from polymers to nanoparticles, Polymers (Basel) 12 (2020) doi:10.3390/polym12051069.

[3] S. Al-Hajri, S.M. Mahmood, A. Abdulrahman, H. Abdulelah, S. Akbari, N. Saraih, An experimental study on hydrodynamic retention of low and high molecular weight sulfonated polyacrylamide polymer, Polymers (Basel) 11 (2019) doi:10.3390/polym11091453.

[4] G. Herth, L. Schornick, F. Buchholz, Polyacrylamides and Poly(Acrylic Acids), in: Ullmann's Encyclopedia of Industrial Chemistry; Wiley-VCH: Weinheim, Germany, 2015; pp. 1-16.

[5] A. Beteta, L. Nurmi, L. Rosati, S. Hanski, K. McIver, K. Sorbie, S. Toivonen, Polymer Chemical Structure and its Impact on EOR Performance, in Proceedings of the SPE Improved Oil Recovery Conference, Tulsa, OK, USA, 2020.

[6] K. Godwin Uranta, S. Rezaei-Gomari, P. Russell, F. Hamad, Studying the effectiveness of polyacrylamide (PAM) application in hydrocarbon reservoirs at different operational conditions, Energies 11 (2018) doi:10.3390/en11092201.

[7] J.H. Lew, P.F. Luckham, O.K. Matar, E.A. Müller, A.S. Santos, M.T. Maung Maung, Consolidation of calcium carbonate using polyacrylamides with different chemistries, Powders 3 (2023) 1–16, https://doi.org/10.3390/powders3010001.

[8] J.H. Lew, O.K. Matar, E.A. Muller, M.T.M. Maung, P.F. Luckham, Adsorption of hydrolysed polyacrylamide onto calcium carbonate, Polymers (Basel) 14 (2022), https://doi.org/10.3390/polym14030405.

[9] K.Y. Hue, J.H. Lew, M.M. Myo Thant, O.K. Matar, P.F. Luckham, E.A. Müller, Molecular dynamics simulation of polyacrylamide adsorption on calcite, Molecules 28, 6367 (2023), https://doi.org/10.3390/molecules28176367.

[10] K.Y. Hue, J.H. Lew, O.K. Matar, P.F. Luckham, E.A. Müller, Parametric studies of polyacrylamide adsorption on calcite using molecular dynamics simulation, Molecules 30 (2025), https://doi.org/10.3390/molecules30020285.

[11] X. Yang, Z. Xiong, J. Mao, T. Yang, B. Fu, D. Han, J. Yang, W. Chen, W. Liu, Q. Zhang, et al., Molecular dynamics simulations to study the adsorption damage of modified polyacrylamide in sandstone pores, J. Mol. Liq. 397 (2024), https://doi.org/10.1016/j.molliq.2024.124096.

[12] X. Ma, X. Sun, M. Chang, Q. Liu, X. Dong, Y. Fan, R. Chen, Adsorption of different ionic types of polyacrylamide on montmorillonite surface: insight from QCM-D and molecular dynamic simulation, Molecules 28 (2023), https://doi.org/10.3390/molecules28114417.

[13] B. Meghwal, N. Rampal, A. Malani, Investigation of adhesion between heavy oil/bitumen and reservoir rock: a molecular dynamics study, Energy Fuel 34 (2020) 16023–16034, https://doi.org/10.1021/acs.energyfuels.0c02921.

[14] G. Xu, H. Wang, Study of cohesion and adhesion properties of asphalt concrete with molecular dynamics simulation, Comput. Mater. Sci 112 (2016) 161–169, https://doi.org/10.1016/j.commatsci.2015.10.024.

[15] P. Badwaik, S. Chobe, A. Malani, Computational study of asphaltene adsorption on carbonate surface: role of molecular structure and oil phase, Energy Fuel 38 (2024) 17355–17369, https://doi.org/10.1021/acs.energyfuels.4c01744.

[16] H. Li, H. Vovusha, S. Sharma, N. Singh, U. Schwingenschlögl, Modeling of n-alkanes on calcite/dolomite by molecular dynamics simulations and first-principles calculations, Adv. Theor. Simul. 4 (2021), https://doi.org/10.1002/adts.202100226.

[17] S. Ren, X. Liu, P. Lin, Y. Gao, S. Erkens, Review on the diffusive and interfacial performance of bituminous materials: From a perspective of molecular dynamics simulation, J. Mol. Liq. 366 (2022), https://doi.org/10.1016/j.molliq.2022.120363.

[18] G.T. Gray, P.J. Maudlin, L.M. Hull, Q.K. Zuo, S.-R. Chen, Predicting material strength, damage, and fracture The synergy between experiment and modeling, J. Fail. Anal. Prev. 5 (2005) 7–17, https://doi.org/10.1361/15477020523725.

[19] G. Xu, H. Wang, Molecular dynamics study of interfacial mechanical behavior between asphalt binder and mineral aggregate, Constr. Build. Mater. 121 (2016) 246–254, https://doi.org/10.1016/j.conbuildmat.2016.05.167.

[20] S. Yang, F. Gao, J. Qu, A molecular dynamics study of tensile strength between a highly-crosslinked epoxy molding compound and a copper substrate, Polymer 54 (2013) 5064–5074, https://doi.org/10.1016/j.polymer.2013.07.019.

[21] P.A.T. Olsson, E. Bergvall, Atomistic investigation of functionalized polyethylene-alumina interfacial strength and tensile behaviour, Comput. Mater. Sci 187 (2021), https://doi.org/10.1016/j.commatsci.2020.110075.

[22] S. Zhou, N. Vu-Bac, B. Arash, H. Zhu, X. Zhuang, Interface characterization between polyethylene/ silica in engineered cementitious composites by molecular dynamics simulation, Molecules 24 (2019), https://doi.org/10.3390/molecules24081497.

[23] D. Sun, Y. Zheng, J. Yan, Y. Wang, J. Wang, Z. Wang, Z. Chen, Y. Cai, S. Cui, M. Lan, et al., Uniaxial tensile deformation and fracture process of structures forming by unsaturated intercalation of amine molecule into C-S-H gel, J Mol Model 28 (2022) 29, https://doi.org/10.1007/s00894-021-04998-5.

[24] K. Ji, C. Arson, Tensile strength of calcite/HMWM and silica/HMWM interfaces: A molecular dynamics analysis, Constr. Build. Mater. 251 (2020), https://doi.org/10.1016/j.conbuildmat.2020.118925.

[25] S.J. Nikkhah, M.R. Moghbeli, S.M. Hashemianzadeh, Dynamic study of deformation and adhesion of an amorphous polyethylene/graphene interface: a simulation study, Macromol. Theory Simul. 25 (2016) 533–549, https://doi.org/10.1002/mats.201600069.

[26] S. Javan Nikkhah, M.R. Moghbeli, S.M.A. Hashemianzadeh, molecular simulation study on the adhesion behavior of a functionalized polyethylene-functionalized graphene interface, Phys Chem Chem Phys 17 (2015) 27414–27427, https://doi.org/10.1039/c5cp04699h.

[27] J. Jose, N. Swaminathan, Interfacial strength cross-over across silica- and graphite-cis-1,4-polyisoprene interfaces, J. Appl. Phys. 123 (2018) 245306, https://doi.org/10.1063/1.5020776.
[28] V. Modi, A.J. Karttunen, Molecular dynamics simulations on the elastic properties of polypropylene bionanocomposite reinforced with cellulose nanofibrils, Nanomaterials (Basel) 12 (2022), https://doi.org/10.3390/nano12193379.
[29] K. Boudraa, T. Bouchaour, Investigating physical behavior of polyacrylamide/polyacrylic acid interpenetrating polymer networks through atomistic molecular dynamics simulations, Mech. Soft Mater. 3 (2021), https://doi.org/10.1007/s42558-021-00038-7.
[30] Z. Yuan, Z. Lu, Z. Yang, J. Sun, F. Xie, A criterion for the normal properties of graphene/polymer interface, Comput. Mater. Sci 120 (2016) 13–20, https://doi.org/10.1016/j.commatsci.2016.04.006.
[31] A.P. Awasthi, D.C. Lagoudas, D.C. Hammerand, Modeling of graphene–polymer interfacial mechanical behavior using molecular dynamics, Model. Simul. Mater. Sci. Eng. 17 (1) (2009) 015002, https://doi.org/10.1088/0965-0393/17/1/015002.
[32] B. Arash, Q. Wang, V.K. Varadan, Mechanical properties of carbon nanotube/polymer composites, Sci. Rep. 4 (2014) 6479, https://doi.org/10.1038/srep06479.
[33] Y. Zhang, X. Zhuang, J. Muthu, T. Mabrouki, M. Fontaine, Y. Gong, T. Rabczuk, Load transfer of graphene/carbon nanotube/polyethylene hybrid nanocomposite by molecular dynamics simulation, Compos. B Eng. 63 (2014) 27–33, https://doi.org/10.1016/j.compositesb:2014.03.009.
[34] P. Demianenko, B. Minisini, G. Ortelli, M. Lamrani, F. Poncin-Epaillard, Computing thermomechanical properties of dry homopolymers used as raw materials for formulation of biomedical hydrogels, J. Mol. Model 22 (2016) 159, https://doi.org/10.1007/s00894-016-3026-9.
[35] Q. Wei, Y. Wang, Y. Che, M. Yang, X. Li, Y. Zhang, Molecular mechanisms in compatibility and mechanical properties of polyacrylamide/polyvinyl alcohol blends, J. Mech. Behav. Biomed. Mater. 65 (2017) 565–573, https://doi.org/10.1016/j.jmbbm.2016.09.011.
[36] Q. Wei, Y. Wang, Y. Rao, A. Jiang, K. Zhang, T. Lu, X. Chen, Evaluating the effects of nanosilica on mechanical and tribological properties of polyvinyl alcohol/polyacrylamide polymer composites for artificial cartilage from an atomic level, Polymers (Basel) 11 (2019), https://doi.org/10.3390/polym11010076.
[37] T. Takada, Y. Morikawa, Y. Kikuchi, D. Miyamoto, Y. Hayasaka, S. Abe, Mechanical and swelling properties of polyacrylamide/polyacrylic acid composite hydrogels: The effects of network structure and carbon nanotube reinforcement, Carbon Reports 3 (2024) 29–36, https://doi.org/10.7209/carbon.030103.
[38] M.I. Voronova, O.V. Surov, A.V. Afineevskii, A.G. Zakharov, Properties of polyacrylamide composites reinforced by cellulose nanocrystals, Heliyon 6 (2020) e05529, https://doi.org/10.1016/j.heliyon.2020.e05529.
[39] L. Pu, Z. Yuan, Y. Cai, X. Li, Z. Xue, Y. Niu, Y. Li, S. Ma, W. Xu, Multiperformance PAM/PVA/CaCO(3) hydrogel for flexible sensing and information encryption, ACS Appl. Mater. Interfaces 16 (2024) 32762–32772, https://doi.org/10.1021/acsami.4c06282.
[40] H. Du, T. Yuan, R. Zhao, M. Hirsch, M. Kessler, E. Amstad, Reinforcing hydrogels with in situ formed amorphous CaCO(3), Biomater. Sci. 10 (2022) 4949–4958, https://doi.org/10.1039/d2bm00322h.
[41] S.-N. Li, B. Li, Z.-R. Yu, S.-W. Dai, S.-C. Shen, M. Mao, L.-X. Gong, Y. Feng, D. Jia, Y. Zhou, et al., Mechanically robust polyacrylamide composite hydrogel achieved by integrating lamellar montmorillonite and chitosan microcrystalline structure into covalently cross-linked network, ACS Appl. Polym. Mater. 2 (2020) 1874–1885, https://doi.org/10.1021/acsapm.0c00106.
[42] D. Hossain, M.A. Tschopp, D.K. Ward, J.L. Bouvard, P. Wang, M.F. Horstemeyer, Molecular dynamics simulations of deformation mechanisms of amorphous polyethylene, Polymer 51 (2010) 6071–6083, https://doi.org/10.1016/j.polymer.2010.10.009.
[43] D. Materials, MedeA 3.5 (Materials Exploration and Design Analysis). 2022.
[44] S. Plimpton, Fast parallel algorithms for short-range molecular dynamics, J. Comput. Phys. 117 (1995) 1–19, https://doi.org/10.1006/jcph.1995.1039.
[45] M.J. Tillotson, N.I. Diamantonis, C. Buda, L.W. Bolton, E.A. Müller, Molecular modelling of the thermophysical properties of fluids: expectations, limitations, gaps and opportunities, Phys Chem Chem Phys (2023), https://doi.org/10.1039/d2cp05423j.
[46] R.W. Hockney, J.W. Eastwood, Computer simulation using particles, Adam Hilger, New York, 1989.
[47] G.J. Martyna, D.J. Tobias, M.L. Klein, Constant pressure molecular dynamics algorithms, J. Chem. Phys. 101 (1994) 4177–4189, https://doi.org/10.1063/1.467468.
[48] L.J. Abbott, K.E. Hart, C.M. Colina, Polymatic: a generalized simulated polymerization algorithm for amorphous polymers, Theor. Chem. Acc. 132 (2013), https://doi.org/10.1007/s00214-013-1334-z.
[49] P. Banerjee, S. Roy, N. Nair, Coarse-grained molecular dynamics force-field for polyacrylamide in infinite dilution derived from iterative boltzmann inversion and MARTINI force-field, J. Phys. Chem. B 122 (2018) 1516–1524, https://doi.org/10.1021/acs.jpcb.7b09019.
[50] P. Banerjee, Development of coarse-grained molecular models of aqueous polyacrylamide, Indian Institute Of Science Education And Research Pune, Bangalore, India, 2016.
[51] J. Koyanagi, N. Takase, K. Mori, T. Sakai, Molecular dynamics simulation for the quantitative prediction of experimental tensile strength of a polymer material, Composites, Part C: Open Access 2 (2020), https://doi.org/10.1016/j.jcomc.2020.100041.
[52] M.M. Thomas, J.A. Clouse, J.M. Longo, Adsorption of organic compounds on carbonate minerals. Model compounds and their influence on mineral wettability, Chem. Geol. 109 (1993) 201–213.
[53] J.H. Lew, K.Y. Hue, O.K. Matar, E.A. Müller, P.F. Luckham, A.S. Santos, M.M. Myo Thant, Atomic force microscopy and molecular dynamic simulation of adsorption of polyacrylamide with different chemistries onto calcium carbonate, Polymers (Basel) 16 (2024), https://doi.org/10.3390/polym16040494.